

Heterogeneous porous media as multiscale structures for maximum flow access

Sylvie Lorente

Laboratoire Matériaux et Durabilité des Constructions, Département de Génie Civil, Institut National des Sciences Appliquées, 135 Avenue de Rangueil, 31077 Toulouse, France

Adrian Bejan^{a)}

Department of Mechanical Engineering and Materials Science, Duke University, Durham, North Carolina 27708-0300

(Received 22 August 2006; accepted 13 September 2006; published online 7 December 2006)

Natural porous structures are heterogeneous with multiple scales that are distributed nonuniformly. Few large pores (fissures, channels, and cracks) are accompanied by numerous finer channels. Can this type of flow architecture be attributed to a principle of maximization of global flow access? Features similar to those of multiscale porous structures are exhibited by tree-shaped flow structures. Trees have been deduced from the maximization of flow access between a point and a volume, a point and an area, and a point and a curve (e.g., circle). In this paper we invoke the same principle and consider fundamentally the question of how to bathe with minimal flow resistance a microchannel structure that globally behaves as a porous medium. We develop completely multiscale configurations that guide the flow from one side of the porous structure to the other (line to line and plane to plane) and show analytically the advantages of tree structures over the usual stacks of parallel microchannels. The “porous medium” that has tree-shaped labyrinths is heterogeneous, with multiple scales that are distributed nonuniformly. These features justify comparisons with the design of natural porous structures. © 2006 American Institute of Physics. [DOI: 10.1063/1.2396842]

I. INTRODUCTION

Tree-shaped flow structures have multiple scales that are distributed nonuniformly through the flow space. Tree flows are everywhere in natural flow systems, and their occurrence can be deduced based on a physics principle [the constructal law:^{1,2} for a flow system to persist in time (to survive) it must evolve in such a way that it provides easier and easier access to the currents that flow through it]. The constructal law has become an addition to the thermodynamics of nonequilibrium systems: the thermodynamics of flow systems with configuration.^{3,4}

Natural porous flow structures also exhibit multiple scales and nonuniform distribution of length scales through the available space. Can such heterogeneous flow structures be derived from the same principle of maximization of flow access? In this paper we explore this possibility by relying on the same deterministic principle as in the study of tree-shaped flow architectures.

Several classes of natural flow configurations are fingerprints of the action of the constructal law. For example, tubes with round cross section are the best (constructal) architecture for flowing from point to point. The corresponding constructal architecture for flowing from one point (source or sink) to an infinity of points (line, area, and volume) is a tree.¹ The tree architecture has multiple scales, which are arranged hierarchically and distributed nonuniformly through the available flow space. The large channels are few and the

small channels are many. Nonuniform distribution of scales means that on the available flow domain there is one place for the trunk and another for the canopy.

Constructal flow configurations constitute a fast growing body of work, which has two major thrusts. One relies on the constructal law to predict and explain the occurrence of natural flow patterns in animate and inanimate systems.^{2,5} The other uses the constructal law as a scientific principle in engineering design.^{2,6} This second thrust of “design as science” forms the subject of this article.

Special among the engineered flow architectures derived from the constructal law are the tree-shaped (dendritic) designs. The growing interest in these flow architectures is illustrated in Refs. 7–22, which were published during the last year or so. The reason is that the multiple scales and optimized (finite) complexity of tree-shaped flows promise greater heat and mass transfer densities with less flow resistance. This principle-based approach guides us to the discovery of lunglike structures for fluid flow and heat and mass transfer.

II. LINE-TO-LINE TREE FLOW

The maximization of flow access between the points of one line and the points of a parallel line can be viewed as a sequence of point-to-line flow access maximization problems (Fig. 1). The building block on which Fig. 1 is based was proposed by Lorente *et al.*,²³ where it was constructed by using optimally shaped rectangular areas, as shown in Fig. 2. Because the pressure drop is proportional to the duct length, the rectangular shape d/c was chosen such that the length of

^{a)}Electronic mail: dalford@duke.edu

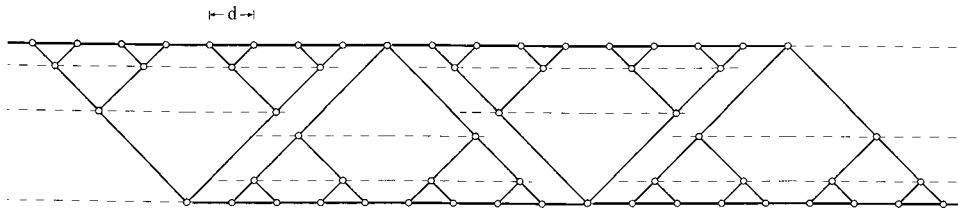


FIG. 1. Tree architecture for connecting the points of one line with the points of another line.

the duct PQ that cuts across the fixed area A_0 is minimum. This yielded the shape $d/c=2$, which led to 90° angles between tributaries and to collinear ducts on the extremities of the V-shaped tree structure.

In this paper, we explore the maximum-access connection between two parallel lines by using the minimum-length shapes of Fig. 2; however, we acknowledge from the start that the 90° angles deduced in Fig. 2 are an approximation of the best (equilibrium^{3,4}) flow structure that could be traced between one point and the many points of a line. To see this, consider the building block sketched in Fig. 3, and abandon the assumption that the stem L_1 and the extreme branch L_2 are collinear. In general, α_1 is not the same as α_2 . The way in which the two branches (or tributaries) cut the upper boundary of the rectangular area S indicates that the Y construct of Fig. 3 is equivalent to a construct that is two-layer thick in Fig. 2.

Assume further that all the tubes are round and with Hagen-Poiseuille flow, and that they are sufficiently slender so that pressure losses at the junctions can be neglected. In this case, the minimization of the pressure drop across the entire Y-shaped construct (subject to fixed total tube volume) yields the well known Hess-Murray law, according to which the ratio of successive tube diameters is $D_1/D_2=2^{1/3}$, regardless of the way in which the tubes are arranged on S .

The optimization of the tube layout is next and is subjected to holding the area S fixed, while the shape of S may

vary. It has been shown that after the optimized D_1/D_2 ratio is substituted into the global pressure drop expression, the global pressure drop is proportional to the geometric flow resistance group,²⁴

$$R = L_1 + 2^{1/3}L_2. \tag{1}$$

There are two degrees of freedom in the morphing of Fig. 3, the angles α_1 and α_2 , or one angle and the aspect ratio of S . The minimization of R subject to $S=\text{constant}$ is performed numerically, and the results are

$$\alpha_1 = 40.86^\circ, \quad \alpha_2 = 53.11^\circ, \tag{2}$$

and the minimized global resistance factor (1) is

$$R = 1.3235S^{1/2}. \tag{3}$$

How much better is this bent-Y structure (Fig. 3) relative to the 45° structure of Fig. 2? The answer is readily obtainable from Eq. (1), in which we substitute $L_2 = \frac{1}{2}L_1$ and, after some algebra, $L_1 = (2S/3)^{1/2}$,

$$R = (1 + 2^{-2/3})\left(\frac{2}{3}\right)^{1/2} = 1.3309S^{1/2}. \tag{4}$$

Comparing Eq. (4) with Eq. (3) we see that the performance of the simpler (minimum-length) structure of Fig. 2 approaches within 0.5% the performance of the more flexible structure optimized in Fig. 3. Such conclusions are reached

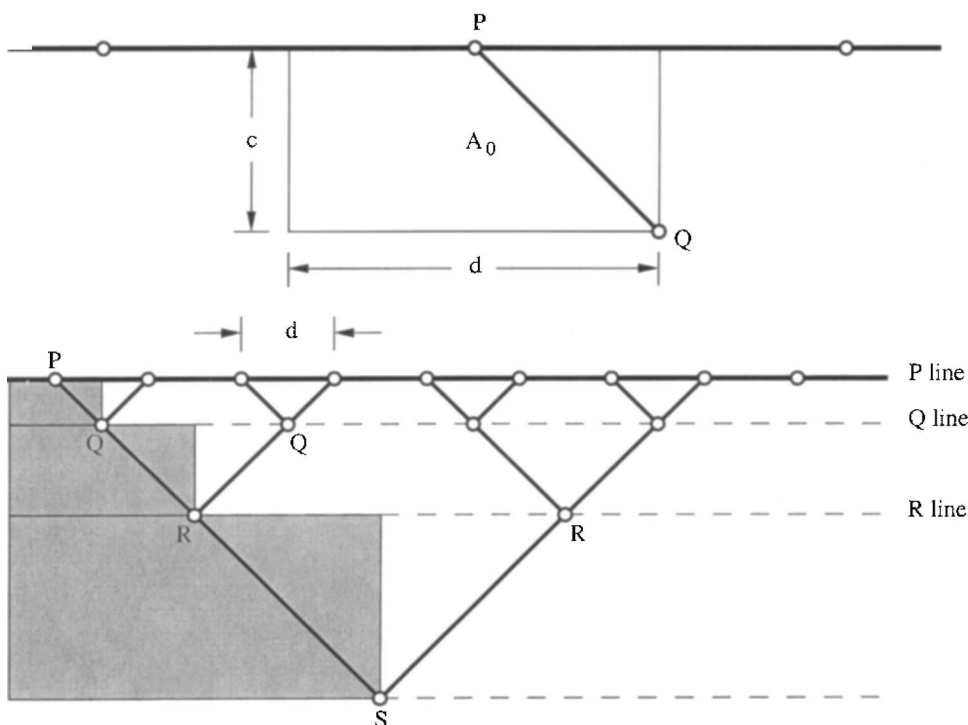


FIG. 2. Tree architecture for connecting one point with one line: the length of every duct is minimized (Ref. 23).

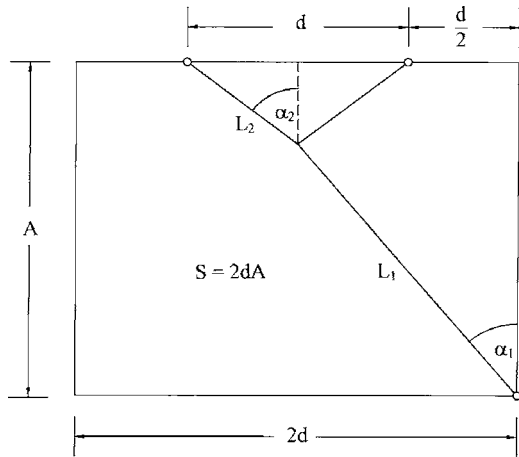


FIG. 3. Y-shaped construct in which, in general, α_1 is not the same as α_2 .

often in constructal theory: optimized nonequilibrium flow architectures come reasonably close to the equilibrium flow architectures. They come close in terms of performance, even though they may look different.

III. TREES OF ROUND TUBES

Because of the comparison made above, in what follows we retain the simpler building blocks sketched in Fig. 2, and with them we explore several ways in which to maximize line-to-line flow access (Fig. 1). Unlike in Fig. 2, we assume a large number of bifurcation levels ($i=1, 2, \dots, n$), as shown in Fig. 4. Because of symmetry about the bisector of the 2α angle, the tube lengths decrease by a factor of $1/2$, from the largest (L_0), to $L_1=L_0/2$, $L_2=L_1/2$, etc. The smallest length scale is the smallest tube length,

$$L_n = 2^{-n}L_0, \tag{5}$$

or the distance between the two ends of two neighboring L_n tubes,

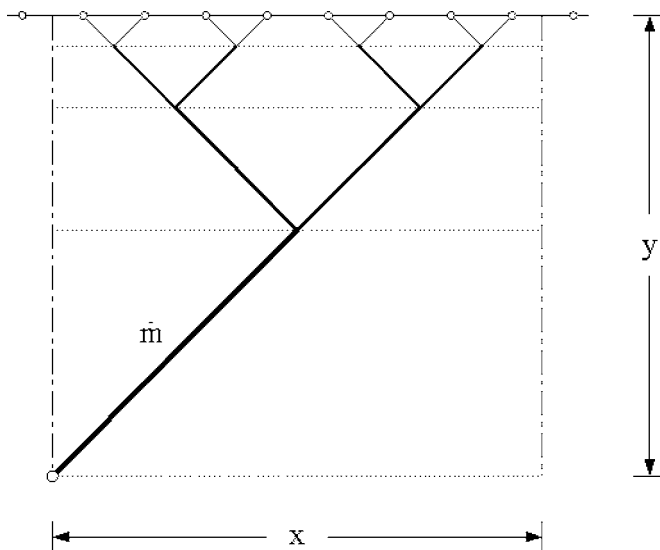


FIG. 4. One of the point-to-line trees of Fig. 1.

$$d = 2L_n \sin \alpha. \tag{6}$$

In this analysis, we carry α as a parameter, although according to the preceding discussion the value of α should be 45° .

The pressure drop along one tube of length L_i and diameter D_i is

$$\Delta P_i = \dot{m}_i \frac{8}{\pi} \text{Po} \nu \frac{L_i}{D_i^4}, \tag{7}$$

where Po is the Poiseuille constant ($\text{Po}=16$ for round tubes), which appears in the formula for the friction factor,

$$f_i = \frac{\text{Po}}{\text{Re}_{D_i}} \tag{8}$$

and $\text{Re}_{D_i} = U_i D_i / \nu$ with $U_i = \dot{m}_i / (\rho \pi D_i^2 / 4)$. Mass conservation at every junction requires that $\dot{m}_i = 2\dot{m}_{i+1}$, where it is again assumed that the tubes are sufficiently slender so that the asymmetry of the Y junction does not affect the splitting of \dot{m}_i into two equal streams \dot{m}_{i+1} . After using the ratios for diameters, lengths, and mass flow rates indicated above, the total pressure drop from the open end of the L_0 tube to the open ends of the L_n tubes becomes

$$\Delta P = \sum_{i=1}^n \Delta P_i = \dot{m}_0 \frac{8}{\pi} \nu \text{Po} \frac{L_0}{D_0^4} \sigma_1, \tag{9}$$

where $\sigma_1 = 1 + 2^{-2/3} + \dots + 2^{-2n/3} = [1 - (2^{-2/3})^{n+1}] / (1 - 2^{-2/3})$. The total tube volume occupied by the tree flow is

$$V = \frac{\pi}{4} (D_0^2 L_0 + 2D_1^2 L_1 + \dots + 2^n D_n^2 L_n) = \frac{\pi}{4} D_0^2 L_0 \sigma_1. \tag{10}$$

The largest length scale (L_0) is related to the vertical dimension of the tree (y) by

$$y = (L_0 + L_1 + \dots + L_n) \cos \alpha = L_0 \sigma_2 \cos \alpha, \tag{11}$$

where $\sigma_2 = 2[1 - 2^{-(n+1)}]$. The horizontal dimension (x) of the area occupied by the tree projection is

$$x = 2^n d = 2L_0 \sin \alpha = \frac{2}{\sigma_2} y \tan \alpha, \tag{12}$$

where 2^n is the number of L_n tubes that reach the upper end of the construct. Eliminating L_0 and D_0 between Eqs. (9)–(11) we obtain

$$\Delta P = \dot{m}_0 \frac{\pi}{2} \text{Po} \frac{\nu}{V^2} \left(\frac{\sigma_1 y}{\sigma_2 \cos \alpha} \right)^3. \tag{13}$$

We question how effective the tree structure of Fig. 4 is relative to a well known reference architecture: an array of N equidistant parallel tubes, each of length y and diameter D . This classical structure carries the same total flow rate \dot{m}_0 in the same total tube volume [$V = N(\pi/4)D^2 y$] and over the same area $xy/2$. The structure has one degree of freedom, the tube diameter D , or the number of parallel tubes,

$$N = \frac{V}{(\pi/4)D^2y}. \quad (14)$$

The pressure drop along this structure (ΔP_{ref}) is the same as the pressure drop along a single tube, cf. Eq. (7), through which the flow rate now is \dot{m}_0/N ,

$$\Delta P_{\text{ref}} = \frac{\dot{m}_0}{N} \frac{8}{\pi} \text{Po} \nu \frac{y}{D^4}. \quad (15)$$

Eliminating D by using Eq. (14) we obtain

$$\Delta P_{\text{ref}} = \dot{m}_0 \frac{\pi}{2} \text{Po} \frac{\nu}{V^2} N y^3. \quad (16)$$

The tree-shaped structure of Fig. 4 has a smaller flow resistance than the parallel channels when $\Delta P < \Delta P_{\text{ref}}$ or, using Eqs. (13) and (16), when

$$N > \left(\frac{\sigma_1}{\sigma_2 \cos \alpha} \right)^3. \quad (17)$$

The right side of this inequality is a number on the order of 1. In conclusion, as the reference structure becomes finer (i.e., as N increases), the tree-shaped design of Fig. 4 becomes more attractive.

This conclusion can be read from the reverse point of view, as a statement of how fine the tree structure must be such that it is preferable to the reference design. For a more practical comparison, assume that the smallest dimension that can be manufactured (d) is the same in both architectures, i.e., the d spacing of Fig. 4 is the same as the spacing between parallel tubes. This means that the number of parallel channels that occupy the area $y(x/2)$ is $N=2^n/2$, and when $\alpha=45^\circ$ the inequality (17) becomes approximately

$$\frac{\Delta P}{\Delta P_{\text{ref}}} \cong \frac{14}{2^n} < 1. \quad (18)$$

We conclude that when the number of branching levels is 4 or larger, the tree-shaped architecture offers greater access to the flow that permeates through the porous structure of thickness y . The superiority of the tree design increases fast as n increases: when $n=7$, the ratio $\Delta P/\Delta P_{\text{ref}}$ is as low as 1/10.

IV. TREES OF TWO-DIMENSIONAL FISSURES

If the tree layout of Fig. 4 consists of fissures that can be modeled as channels between smooth parallel walls of length L_i and spacing D_i , then the preceding analysis can be reconstructed starting with the equivalent of Eq. (7),

$$\Delta P_i = \dot{m}'_i \frac{1}{2} \text{Po} \nu \frac{L_i}{D_i^3}, \quad (19)$$

in which $\text{Po}=24$ for parallel-plate channels and \dot{m}'_i is the mass flow rate per unit length in the direction perpendicular to Fig. 4. The optimal ratio of successive parallel-plate spacings is $D_i/D_{i+1}=2^{1/2}$ (cf. Ref. 24), which is analogous to the Hess-Murray law for successive diameters of bifurcating round tubes. The total pressure drop is

$$\Delta P = \sum_{i=1}^n \Delta P_i = \dot{m}'_0 \frac{1}{2} \text{Po} \nu \frac{L_0}{D_0^3} \sigma_3, \quad (20)$$

where $\sigma_3=2[1-2^{-(n+1)}]$. The total volume occupied by the fissures is $V'=D_0L_0+2D_1L_1+\dots+2^nD_nL_n$, which yields

$$V' = D_0L_0\sigma_3, \quad (21)$$

where $\sigma_3=2[1-2^{-(n+1)/2}]/(1-2^{-1/2})$ and V' is the total flow volume per unit length in the direction perpendicular to Fig. 4. Eliminating L_0 and D_0 between Eqs. (11), (20), and (21) we obtain

$$\Delta P = \frac{\dot{m}'_0 \text{Po} \nu}{2(V')^3} \left(\frac{y\sigma_3}{\sigma_2 \cos \alpha} \right)^4. \quad (22)$$

The reference (classical) design is a stack of N parallel-plate channels of height y and spacing D , covering the two-dimensional space $y(x/2)$. If the channel-to-channel spacing matches the smallest scale of the tree structure (d , Fig. 4), then $N=2^n/2$. For the reference design, we write in order

$$\Delta P_{\text{ref}} = \frac{\dot{m}'_0}{N} \frac{1}{2} \text{Po} \nu \frac{y}{D^3} = \dot{m}'_0 \text{Po} \nu \frac{y^4}{(V')^3} 2^{2n-3}, \quad (23)$$

where $V'=NyD$. By comparing Eqs. (23) and (22) we find that when $\alpha=45^\circ$ the tree structure promises greater access to the flow when

$$\frac{\Delta P}{\Delta P_{\text{ref}}} \cong \frac{2174}{4^n} < 1. \quad (24)$$

The ratio $\Delta P/\Delta P_{\text{ref}}$ is smaller than 1 when n is 6 or greater. This ratio decreases as n increases (e.g., $\Delta P/\Delta P_{\text{ref}} \sim 1/10$ when $n=7$), and this decrease is faster than what we found in the case of trees of tubes in Eq. (18).

The fissured layer of Fig. 1 can be regarded as a porous layer of thickness y and permeability K defined as

$$u = \frac{K \Delta P}{\mu y}, \quad (25)$$

where the volume averaged velocity in the y direction is $u = \dot{m}'_0/(\rho x/2)$. Using Eq. (22) for ΔP , we find that

$$K = \frac{\phi^3}{8\text{Po}} \left(\frac{\sigma_2}{\sigma_3} \right)^4 (y \sin 2\alpha)^2, \quad (26)$$

where ϕ is the porosity of the layer,

$$\phi = \frac{V'}{yx/2}, \quad (27)$$

and $x=y \tan \alpha$. Equation (26) shows that the permeability is maximum when $\alpha=45^\circ$, which coincides with the discussion following the analysis of Fig. 3.

V. CONSOLIDATION OF TREE STRUCTURES

An additional step toward a lower overall ΔP is illustrated in going from Fig. 1 to Fig. 5(a). For better use of the available space, it makes sense to eliminate the spacing d , which in Fig. 1 separates two adjacent trees. This move brings together the extreme arms of two neighboring trees, such that the final configuration [Fig. 5(b)] recommends it-

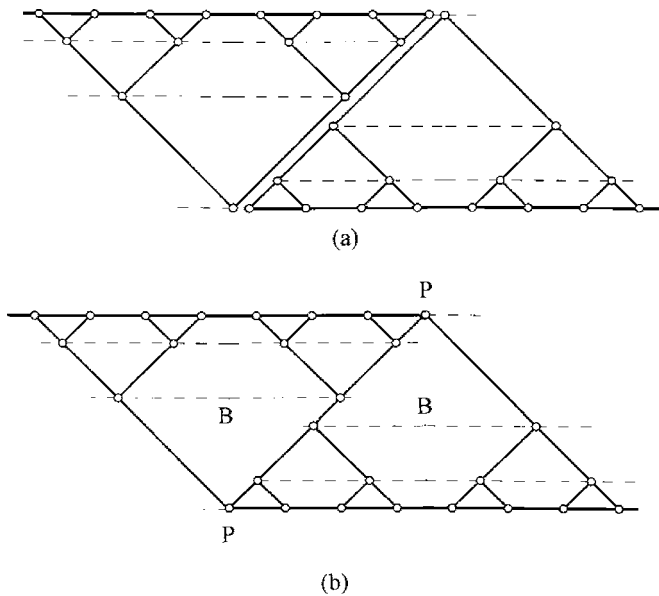


FIG. 5. The compacting of the multitree structure of Fig. 1.

self: the two trees are served by a common extreme arm, which may be thick (D_0) all the way from P to P .

The migration of the flow configuration from Fig. 1 to Fig. 5 is important because it suggests an explanation for the occurrence of large pores and fissures through natural porous structures. These large features are strangely oriented, at an angle, not directly across the porous layer. Now we see why. The large channel P – P has two duties, to carry fluid across the layer directly and to feed the neighboring trees, which also carry fluid across the layer. The appearance of raggedness and disorganization is an illusion: such features come from the same principle as all the other features of the tree drawings.

How beneficial is it to replace Fig. 1 with Fig. 5? We answer this question by considering fixed two global quantities: \dot{m}' , the mass flow rate across the layer, expressed per unit of length in the horizontal direction in Fig. 1; v' , the total duct volume, expressed per unit of length in the horizontal direction in Fig. 1. With reference to Fig. 4, which is one tree (half of the building block of Fig. 1), the total mass flow rate across the block of thickness y and width x is $2\dot{m}_0 = \dot{m}'x$, where $x = 2^n d$, cf. Eq. (12). The total duct volume is $2V = v'x$, where V is given by Eq. (10).

In going from Fig. 1 to Fig. 5, the width of the building block decreases from x to $x-d$. The total mass flow rate for Fig. 5 is $2\dot{m}_5 = \dot{m}'(x-d)$, and the total tube volume is $2V_5 = v'(x-d)$. Combining these relations with the preceding ones for the structure of Fig. 1, we obtain

$$\frac{\dot{m}_5}{\dot{m}_0} = \frac{x-d}{x} = \frac{V_5}{V}. \quad (28)$$

According to Eq. (13), the overall pressure drop is proportional to \dot{m}_0/V^2 , which means $(\dot{m}'x)/(v'x)^2$, or x^{-1} . The pressure drop across the layer of Fig. 5 varies as $\dot{m}'(x-d)/[v'(x-d)]^2$ or $(x-d)^{-1}$. In conclusion, from Fig. 1 to Fig. 5 the global pressure drop of the layer increases by the factor $x/(x-d) = (1-2^{-n})^{-1}$, which is essentially 1 when n

exceeds 4. Although the structure of Fig. 5 is marginally less permeable (this is another confirmation of the earlier work done on trees, Figs. 2 and 3), Fig. 5 is simpler than Fig. 1. It has fewer channels: this is an attractive feature for the design of microchannel structures.

VI. PLANE-TO-PLANE TREES

Further developments along the conceptual path outlined in this paper are possible if we explore the three-dimensional counterparts of Figs. 1–5. Instead of line-to-line trees, in Fig. 6 we show schematically the use of three-dimensional trees to facilitate the flow between two parallel planes. Instead of the building block (single tree) that connects one segment of one line with one point on the opposite line (Fig. 1), now we consider the building block shown in Fig. 7: a triangular patch in the bottom plane is to be connected to one point in the upper plane. Forests of such trees will be interspaced with their upside-down counterparts to connect the two planes with less resistance than a bundle of parallel tubes using the same tube volume.

The opportunity to discover the best architecture of a point-to-plane tree is illustrated by the following analysis of the construct of Fig. 7. A tube of length L_1 and diameter D_1 splits into three identical tubes of lengths L_2 and diameters D_2 . Mass conservation requires $\dot{m}_1 = 3\dot{m}_2$. If the total tube volume is fixed,

$$V = L_1 D_1^2 + 3L_2 D_2^2, \quad (29)$$

we can show that the overall pressure drop,

$$\Delta P \sim \dot{m}_1 \frac{L_1}{D_1^4} + \dot{m}_2 \frac{L_2}{D_2^4}, \quad (30)$$

is minimum when

$$\frac{D_2}{D_1} = 3^{-1/3}. \quad (31)$$

Substituting $\dot{m}_2/\dot{m}_1 = 1/3$ and Eq. (31) into Eq. (30), we conclude that the minimized global flow resistance depends on geometry as follows:

$$\frac{\Delta P}{\dot{m}} \sim \frac{1}{D_1^4} (L_1 + 3^{1/3} L_2). \quad (32)$$

The corresponding total tube volume is

$$V = D_1^2 (L_1 + 3^{1/3} L_2), \quad (33)$$

such that Eq. (32) becomes

$$\frac{\Delta P}{\dot{m}} \sim \frac{1}{V^2} (L_1 + 3^{1/3} L_2)^3. \quad (34)$$

The quantity to minimize further is $(L_1 + 3^{1/3} L_2)$. We do this by optimizing the three-dimensional structure shown in Fig. 7. The three L_2 tubes meet at a point inside the pyramid, which is located at the distance h above the base plane. The height of the pyramid is $H = L_1 + h$. The base is an equilateral triangle. The projections of the L_2 tubes on the base meet in

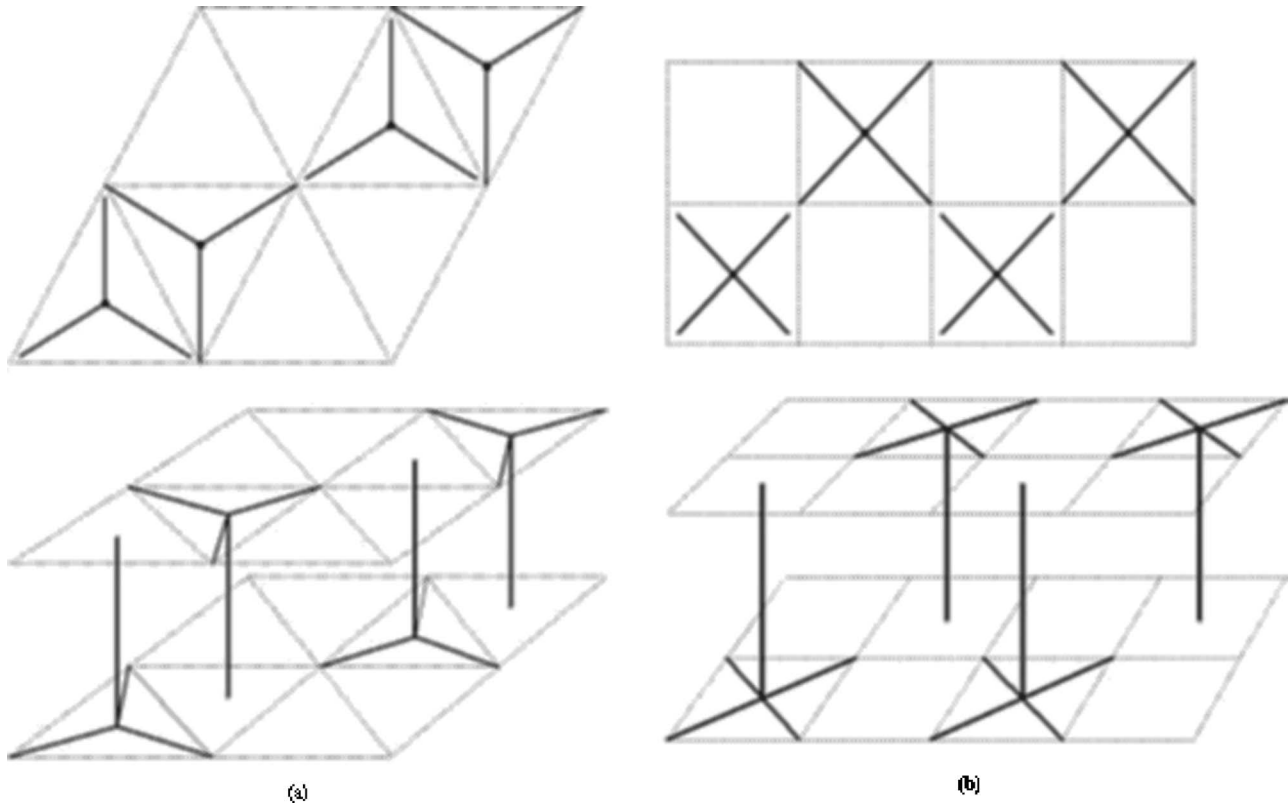


FIG. 6. Conceptual tree architecture for connecting the points of one plane with the points of a parallel plane.

the center of the base. One can show that the base area is equal to $(3^{3/2}/4)(L_2^2 - h^2)$, and that the volume of the entire pyramid is

$$V_p = \frac{3^{1/2}}{4}(h + L_1)(L_2^2 - h^2). \tag{35}$$

We illustrate the optimization of the flow structure in two scenarios. In the first, the total volume of the structure (V_p) is fixed, and we seek not only the best tripodal structure but also the shape of the V_p pyramid. According to the method of Lagrange multipliers, to minimize expression (6) subject to the constraint (7) is the same as minimizing the aggregate function,

$$\Phi = L_1 + 3^{1/3}L_2 + \lambda(h + L_1)(L_2^2 - h^2), \tag{36}$$

where λ is the Lagrange multiplier. Solving the system $\partial\Phi/\partial L_1=0$ and $\partial\Phi/\partial L_2=0$, we obtain

$$\frac{2}{3^{1/3}} \frac{L_1}{L_2} \left(1 + \frac{h}{L_1}\right) = 1 - \left(\frac{h}{L_1}\right)^2 \left(\frac{L_1}{L_2}\right)^2. \tag{37}$$

This yields the optimal ratio L_1/L_2 as a function of the position of the tube junction, h/L_1 . If we make the assumptions

$$\frac{L_1}{L_2} \sim 1, \tag{38}$$

$$\varepsilon = \frac{h}{L_1} \ll 1, \tag{39}$$

then on the right side of Eq. (37) we may neglect the $(h/L_1)^2$ term. The optimal length ratio reduces to

$$\frac{L_1}{L_2} = \frac{3^{1/3}}{2(1 + \varepsilon)} \leq 1. \tag{40}$$

The pyramid volume (41) becomes

$$V_p = 3^{-1/6} L_1^3 (1 + \varepsilon)^3. \tag{41}$$

The global flow resistance factor $(L_1 + 3^{1/3}L_2)$ becomes

$$L_1 + 3^{1/3}L_2 = L_1 \left(1 + 3^{1/3} \frac{L_2}{L_1}\right) = 3^{1/18} V_p^{1/3} \frac{3 + 2\varepsilon}{1 + \varepsilon}. \tag{42}$$

This function decreases monotonically as ε decreases and reaches its lowest value at $\varepsilon=0$, which means

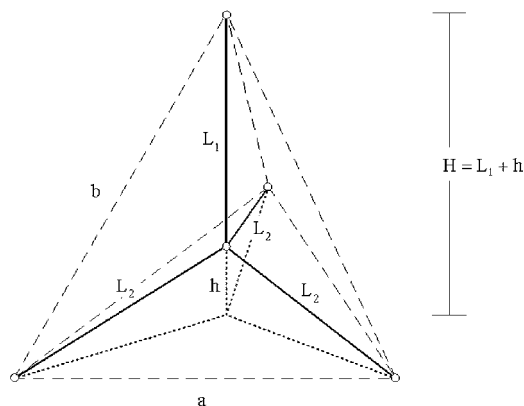


FIG. 7. Tripod for connecting one point of one plane with three points in the opposite plane.

$$h=0 \text{ and } \frac{L_1}{L_2} = \frac{3^{1/3}}{2}. \quad (43)$$

These values confirm the validity of the simplifying assumptions made in Eqs. (38) and (39).

In conclusion, the best way to configure in three dimensions a tube that splits into three identical tubes, such that the resulting tree fills a pyramid of fixed size, is to make L_1 the height of the pyramid and L_2 the segments linking the center of the base (an equilateral triangle) with the three corners of the base. In this scenario, the pyramid has an optimal shape indicated by the ratio $L_1/L_2=3^{1/2}/2$. This elemental structure was used in Fig. 6 to illustrate the filling of the porous space between the two planes.

In the second scenario we assume that the height of the pyramid H is fixed. This dimension accounts for the thickness of the heterogeneous porous layer, which in Fig. 6 is the distance between the upper and lower planes. We also fix the side (a) of the equilateral triangle, which serves as base. This means that the lateral edge of the pyramid has a fixed length (b), which in the following analysis is used as length scale. The optimization of the tripodal flow structure reduces to finding the aspect ratios L_2/b or L_1/b . The geometric relation between the two aspect ratios is

$$\lambda_1 = g - (\lambda_2^2 - 1 + g^2)^{1/2}, \quad (44)$$

where $\lambda_1=L_1/b$, $\lambda_2=L_2/b$, and $g=H/b$. In place of Eq. (34), the global flow resistance emerges as a function of λ_1 and λ_2 ,

$$\frac{\Delta PV^2}{mb^3} \sim (3^{-1/3}\lambda_1 + \lambda_2)^3 = R. \quad (45)$$

In view of the constraint (44), the flow resistance R is a function of λ_2 and g . Two regions of this surface are accessible and analytical. If $L_1=0$, the L_2 tubes start from the top of the pyramid ($L_2=b$), and $R=1$. The opposite extreme is when the tripod has a flat base [e.g., Fig. 7, $L_2=(b_2-H_2)^{1/2}$], which means that

$$R = [3^{-1/3}g + (1 - g^2)^{1/2}]^3. \quad (46)$$

This function is greater than 1 when $g < 0.937$ or $H < 0.937b$. In this range, the design with $L_1=0$ (or $L_2=b$) is superior. For example, when $H/b=0.8$, Eq. (46) yields $R=3.44$. Only when the pyramid is very slender ($0.937 < H/b < 1$) is the tripod with flat foot (Fig. 7) the recommended flow structure.

VII. CONCLUSIONS

In this paper we invoked the maximization of flow access through a porous medium that has a freely morphing flow structure. We considered two-dimensional structures (line-to-line flow) and three-dimensional structures (plane-to-plane flow). The flow architectures that resulted are assemblies of tree-shaped flow building blocks. Each assembly is a sequence in which upright trees alternate with downright trees. The flow is in the same direction through both types of trees, for example, vertically downward in Fig. 6.

The chief conclusion is that these alternating-tree architectures have flow resistances that are lower than those of

porous media with the same volume and internal (duct) flow volume. These architectures have multiple scales that are arranged hierarchically, because every tree is an optimized multiscale flow structure. The observer who looks from the outside at the side of the porous medium (e.g., from the top of Figs. 1 and 6) sees a few large pores surrounded by many small pores. From this viewing position, the porous medium appears to have two scales.

The structural properties uncovered in this study are qualitatively the same as those of natural porous materials²⁵ [e.g., the soil of the hill slope in a river drainage basin, where two scales dominate: fine porous soil with seepage and larger pores (“pipes”) embedded in the fine structure]. At this stage in our investigation, we report as very promising the similarities that emerge between natural porous structures and the ones derived from principle. Future work could examine more quantitatively the similarities between the natural and the deduced architectures. Such work may shed light on the natural process that *generates* multiple scales and heterogeneity in flow systems such as hill slope drainage and living tissues.

Promising in this respect is the coincidence that in a recent computational simulation²⁶ of the generation of vasculature through a slab-shaped tissue with deformable internal structure, the simulations lead to a structure of alternating trees similar to what we proposed in Fig. 1. The tissue deformation model used in Ref. 26 is similar to the drainage basin erosion model of Ref. 27, where the emerging flow architecture was a single tree because in a drainage basin the flow is from an area to one point, not from one area to another area (Figs. 1 and 6). The recent progress on the “constructal” theory and design of flow architectures for greater and greater flow access is reviewed in Ref. 28.

¹A. Bejan, *Advanced Engineering Thermodynamics*, 2nd ed. (Wiley, New York, 1997).

²A. Bejan, *Shape and Structure, from Engineering to Nature* (Cambridge University Press, Cambridge, UK, 2000).

³A. Bejan and S. Lorente, *Int. J. Heat Mass Transfer* **4**, 3203 (2004).

⁴A. Bejan and S. Lorente, *La Loi Constructale* (L'Harmattan, Paris, 2005).

⁵A. Bejan, *J. Exp. Biol.* **208**, 1677 (2005).

⁶A. Bejan, I. Dincer, S. Lorente, A. F. Miguel, and A. H. Reis, *Porous and Complex Flow Structures in Modern Technologies* (Springer, New York, 2004).

⁷G. Hernandez, J. K. Allen, and F. Mistree, *Eng. Optimiz.* **35**, 229 (2003).

⁸H. Brod, *J. Non-Newtonian Fluid Mech.* **111**, 107 (2003).

⁹D. Tondeur and L. Luo, *Chem. Eng. Sci.* **59**, 1799 (2004).

¹⁰L. Gosselin, *Int. J. Heat Mass Transfer* **48**, 2159 (2005).

¹¹Y. Chen and P. Cheng, *Int. Commun. Heat Mass Transfer* **32**, 931 (2005).

¹²A. Y. Alharbi, D. V. Pence, and R. N. Cullion, *J. Fluids Eng.* **125**, 1051 (2003).

¹³A. D. Kraus, ASME International Mechanical Engineering Congress and Exposition, Washington, DC, 2003.

¹⁴G. F. Jones and S. Ghassemi, ASME Heat Transfer/Fluids Engineering Summer Conference, Charlotte, NC, 11–15 July 2004.

¹⁵S. M. Senn and D. Poulikakos, *J. Power Sources* **130**, 178 (2004).

¹⁶S. M. Senn and D. Poulikakos, *J. Appl. Phys.* **96**, 842 (2004).

¹⁷Y. Azoumah, N. Mazet, and P. Neveu, *Int. J. Heat Mass Transfer* **47**, 2961 (2004).

¹⁸Y. S. Muzychka, *Int. J. Heat Mass Transfer* **48**, 3119 (2005).

¹⁹F. Lundell, B. Thonon, and J. A. Gruss, Second Conference on Microchannels and Minichannels, Rochester, NY, 2004.

- ²⁰M. Lallemand, F. Ayela, M. Favre-Marinet, A. Gruss, D. Maillet, P. Marty, H. Peerhossaini, and L. Tadrist, Congrès Français de Thermique, SFT 2005, Reims, 30 May–2 June 2005.
- ²¹A. K. Pramanick and P. K. Das, *Int. J. Heat Mass Transfer* **48**, 1851 (2005).
- ²²A. K. Pramanick and P. K. Das, *Int. J. Heat Mass Transfer* **48**, 1974 (2005).
- ²³S. Lorente, W. Wechsatoł, and A. Bejan, *Int. J. Heat Mass Transfer* **45**, 3299 (2002).
- ²⁴A. Bejan, L. A. O. Rocha, and S. Lorente, *Int. J. Therm. Sci.* **39**, 949 (2000).
- ²⁵D. A. Nield and A. Bejan, *Convection in Porous Media*, 2nd ed. (Springer, New York, 1999).
- ²⁶D. Szczerba and G. Szekely, *J. Theor. Biol.* **234**, 87 (2005).
- ²⁷M. R. Errera and A. Bejan, *Fractals* **6**, 245 (1998).
- ²⁸A. Bejan and S. Lorente, *J. Appl. Phys.* **100**, 041301 (2006).